

# A FULLY POLARIMETRIC SAR RAW SIGNAL SIMULATOR

*Gerardo Di Martino, Antonio Iodice, Davod Poreh, Daniele Riccio*

Dipartimento di Ingegneria Elettrica e delle Tecnologie dell'Informazione, Università di Napoli Federico II, 80125, Naples, Italy

## ABSTRACT

We present a new Synthetic Aperture Radar (SAR) raw signal simulator, which is able to simultaneously generate the raw signals of the different polarimetric channels of a polarimetric SAR system in such a way that the correct covariance matrix is obtained for the final images. Extended natural scenes, dominated by surface scattering, are considered. A fast Fourier-domain approach is used for the generation of raw signals. Presentation of theory is supplemented by meaningful experimental results.

**Index Terms**— Rough surfaces, Synthetic Aperture Radar (SAR), SAR Polarimetry, SAR simulation.

## 1. INTRODUCTION

In recent years, Synthetic Aperture Radar (SAR) Polarimetry has been successfully applied to soil moisture retrieval, forest monitoring, change detection and marine applications [1]. Therefore, a polarimetric SAR raw signal simulator, based on a sound physical electromagnetic scattering model, would be certainly useful for mission planning, algorithm development and testing, and prediction of suitability of the system to different applications. An efficient simulator with many of the above cited features, called SARAS [2-5], is actually available in literature: in fact, it is a model-based raw signal simulator that, among other system characteristics, also accounts for the transmitting and receiving polarizations. However, it can only simulate one polarimetric channel at a time, with the result that data of different channels turn out to be independent. Accordingly, although the correct relations between channels' powers are obtained, the covariance (or coherence) matrix of the final images is not realistic.

Here we present an updated version of that simulator that is able to simultaneously produce the raw signals of the different polarimetric channels in such a way as to obtain the correct covariance or coherence matrixes on the final images. In the following we will refer to the simulator for the classical stripmap acquisition mode [2], but the same modifications also apply to simulators for spotlight [3] and hybrid [4] acquisition modes, as well as to the one accounting for platform trajectory deviations [5]. In addition, we here only consider surface scattering, but, due

to the modular structure of the simulator, also other scattering mechanisms (volumetric, double bounce) can be included, if reliable models are available.

## 2. THEORY

The SARAS simulator of [2-6] employs a procedure that consists of two main stages. In the first stage, given the orbit and system data and the scene geometric and electromagnetic parameters, the scene reflectivity map is evaluated. In the second stage, the SAR raw signal is computed via a superposition integral in which the reflectivity map is weighted by the SAR system two-dimensional (2D) pulse response. This superposition integral is efficiently evaluated in the Fourier domain via FFT codes. When we move to the polarimetric case, the second stage remains conceptually unchanged, whereas the first one, i.e., reflectivity map evaluation, must be properly changed, as detailed in the following. As in the usual SARAS simulator, the surface macroscopic profile, provided by an external Digital Elevation Model (DEM), is approximated by rectangular rough facets, large with respect to wavelength but smaller than SAR system resolution. However, at variance with the available SARAS, zero-mean random deviations of the facets' azimuth and range slopes, with respect to those prescribed by the external DEM, are added; their standard deviations can be selected by the user to model the large-scale roughness (in addition to the facet small-scale roughness). The reflectivity of each facet can be computed by using the small perturbation method (SPM) or the Physical Optics (PO), according to the facet roughness [6], and it can be expressed as

$$\gamma_{pq}(x, r; \vartheta_l, \beta) = \chi_{pq}(x, r; \vartheta_l, \beta) w(x, r; \vartheta_l) , \quad (1)$$

where, see also Fig.1,  $p$  and  $q$  are the polarizations of the incident and scattered field, respectively, and can each stand for  $H$  (horizontal) or  $V$  (vertical),  $x$  and  $r$  are the azimuth and range coordinates of the facet's center,  $\vartheta_l$  is the local incidence angle (i.e., the angle formed by the look direction and the direction perpendicular to the facet),  $\beta$  is the angle between global and local incidence planes (i.e., between the vertical plane including the look direction, and the plane

perpendicular to the facet and including the look direction),  $\underline{\underline{\chi}}_{pq}$  are the elements of the matrix

$$\underline{\underline{\chi}}_{pq}(\vartheta_l, \beta) = \underline{\underline{R}}_2(\beta) \begin{pmatrix} F_H(\vartheta_l) & 0 \\ 0 & F_V(\vartheta_l) \end{pmatrix} \underline{\underline{R}}_2^{-1}(\beta) \quad (2)$$

$$\underline{\underline{R}}_2(\beta) = \begin{pmatrix} \cos \beta & \sin \beta \\ -\sin \beta & \cos \beta \end{pmatrix} \quad (3)$$

is the  $2 \times 2$  unitary rotation matrix, and  $F_H$  and  $F_V$  are either the Bragg (if SPM is used) or the Fresnel (if PO is used) coefficients for  $H$  and  $V$  polarization, respectively. Finally,  $w(\vartheta_l)$  is a polarization-independent circular Gaussian random variable with zero mean, and variance to be computed according to the employed scattering model [6]: in the SPM case, it is proportional to the power spectral density  $W(\cdot)$  of the facet's roughness:

$$\langle |w(\vartheta_l)|^2 \rangle = k^4 \cos^4 \vartheta_l W(2k \sin \vartheta_l) \quad (4)$$

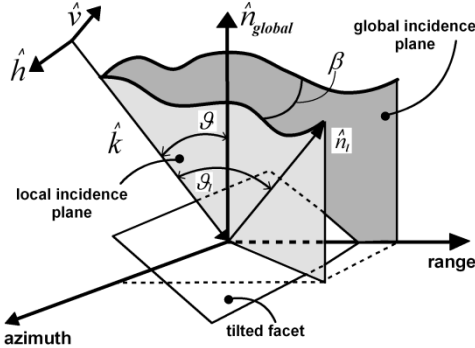


**Fig. 1.** Facet's  $\vartheta_l$  and  $\beta$  angles.

where  $k$  is the wavenumber; for the PO case, see [6] and references therein. At variance with the already available simulator, in this updated version the three polarimetric channels  $HH$ ,  $VV$  and  $HV=VH$  ( $HV$  and  $VH$  coincide, due to reciprocity) are simulated at the same time, and the same realization of the random variable  $w(\vartheta_l)$  is used for the three channels. This ensures that the polarimetric channels are not independent; on the other hand, the randomness of the facet slopes (which causes the randomness of local incidence and  $\beta$  angles) introduces a decorrelation among the different channels. The corresponding computed coherency matrix is in agreement with theoretical predictions, when they are available, as shown in the next Section.

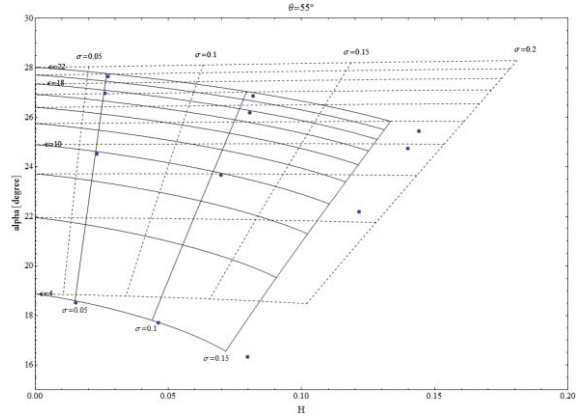


**Fig. 2.**  $H\text{-}\alpha$  graphs comparison with PTSM and X-Bragg.

### 3. SIMULATION RESULTS

Here we report some of the results obtained using the proposed simulator by setting system parameters similar to those of the L-band PALSAR sensor. In Fig. 2 we show the coherency matrix entropy-alpha graphs [7] obtained from simulated images (blue dots) of a flat scene with random facets slopes, whose standard deviations (equal for range and azimuth) vary from 0 to 0.2, and compare them with theoretical ones obtained by using the PTSM [6] (solid line) and X-Bragg [7] (dashed line) approximated theoretical models. This comparison shows that obtained coherency matrix behavior is more in agreement with what expected from theory, and in particular from PTSM.

In Fig. 3 we show the entropy and alpha images obtained from simulated polarimetric data of a scene with significant topography, namely the area of Mt. Vesuvius, near Naples, Italy.

Furthermore, we provide meaningful results regarding the copol-crosspol and copol-corr graphs generated using PolSARAS simulated images. Copolarized (copol) and crosspolarized (crosspol) ratios and correlation coefficient (corr) are defined as follows:

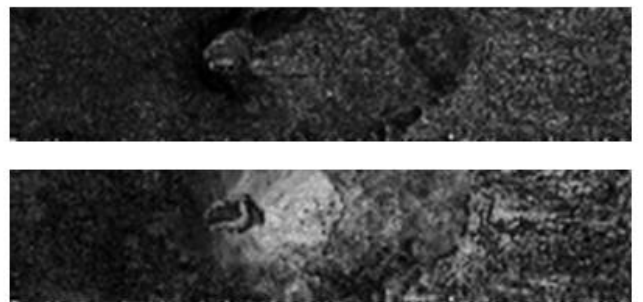


**Fig. 3.** Entropy (top) and alpha angle (bottom) maps for the Vesuvius scene. Near range is on the left.

$$\begin{cases} copol = \frac{\langle |i_{HH}|^2 \rangle}{\langle |i_{VV}|^2 \rangle} \\ crosspol = \frac{\langle |i_{HV}|^2 \rangle}{\langle |i_{VV}|^2 \rangle} \\ corr = \frac{|\langle i_{HH} i_{VV}^* \rangle|}{\sqrt{\langle |i_{HH}|^2 \rangle \langle |i_{VV}|^2 \rangle}} \end{cases} \quad (5)$$

where  $i_{pq}$  are the focused complex images relevant to the  $pq$  polarimetric channel. For PTSM the dependence on small-scale-roughness parameters  $T$  and  $H_t$  cancels out in the ratios in (5), so that these ratios only depend on the large-scale-roughness  $\sigma$  and on the relative dielectric permittivity  $\varepsilon$ . We exploited this to devise a method for the estimation of  $\varepsilon$  from measured polarimetric data: the obtained estimates can be used for the estimation of the volumetric soil moisture, via appropriate mixing models. Pol-SARAS simulations provide the possibility to generate graphs that are not subject to PTSM approximations. In the following, we discuss how the proposed simulator can be used to obtain the abovementioned graphs.

Once the three channels' images were obtained, we evaluated the quantities in (5) using a multilook of  $8 \times 8$  pixels and then averaging over the whole scene. Finally, we repeated the simulations for several values of  $\varepsilon$  and  $\sigma$ , in order to obtain the copol-crosspol and copol-corr graphs. This kind of graphs can be used to generate look-up tables, employed for soil moisture retrieval. One example is given in Fig. 4.

A unique characteristic of the Pol-SARAS simulator is the possibility to account for anisotropic features of terrain roughness. Indeed, in the simulator it is possible to set two different values for the standard deviation of the facets' slopes in range and azimuth directions, i.e.  $\sigma_x \neq \sigma_y$ . This possibility is particularly interesting in case of agricultural applications, where harvesting and vegetation growth can easily impose anisotropy on soil shape. The results for this case are shown in Fig. 5. The simulations parameters are: look angle of  $45^\circ$  and  $\varepsilon = 4$ . In Fig. 5(top), we compare the results obtained for the copol-crosspol graph setting  $\sigma_x = \sigma_y = \sigma$  (i.e., the isotropic case), with those obtained setting  $\sigma_x = 0$  and  $\sigma_y = \sqrt{2} \sigma$ , or  $\sigma_y = 0$  and  $\sigma_x = \sqrt{2} \sigma$  (i.e., two anisotropic cases). The square root of two factor is used to make the graphs comparable, recalling that the overall roughness in the case  $\sigma_x = \sigma_y = \sigma$  can be expressed as  $\sqrt{\sigma_x^2 + \sigma_y^2} = \sqrt{2} \sigma$ . As theoretically expected, since in the absence of azimuth slopes crosspolarization is not present, when  $\sigma_x = 0$  (i.e., only range slope, no azimuth slope), the crosspol ratio is practically zero independently from  $\sigma_y$  value; however, for visualization purposes in Fig.5(top) we set it to the conventional value of -60 dB.

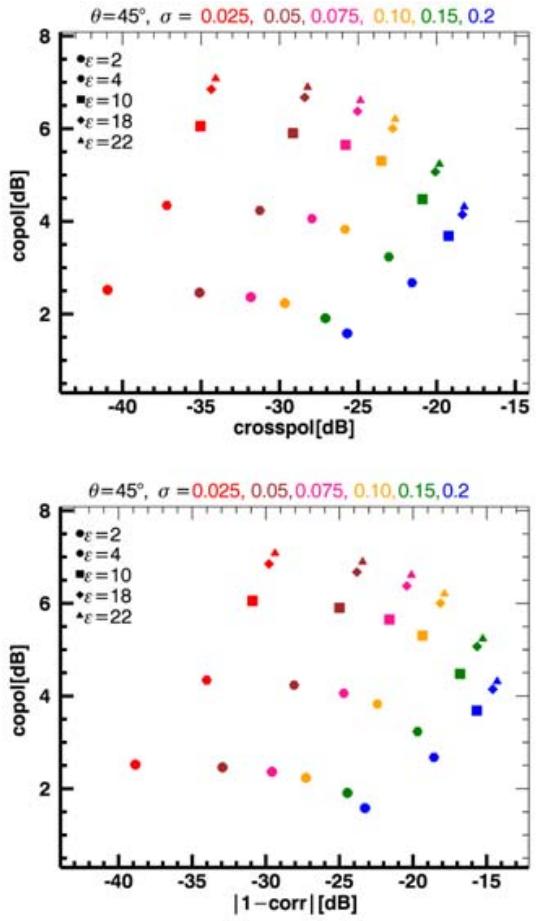


**Fig. 4.** Copol-crosspol (top) and copol-corr (bottom) graphs for  $\theta = 45^\circ$ .

Moreover, we notice that, in this case, the values of copol ratio obtained for a certain  $\sigma$  are slightly lower than those obtained in the case of  $\sigma_x = \sigma_y = \sigma$ . When  $\sigma_y = 0$ , (i.e., only azimuth slope, no range slope) the results are somehow inverted. In particular, the range of variation of the copol ratio is smaller than for the case  $\sigma_x = \sigma_y = \sigma$ ; conversely, the range of the variation of the crosspol ratio is larger than that of the case  $\sigma_x = \sigma_y = \sigma$ . This is due to the high sensitivity of the crosspol ratio to azimuth slopes. From the viewpoint of soil-moisture estimation, i.e. of  $\varepsilon$  estimation, it is evident that in presence of significant anisotropy the estimation is impaired, since  $\varepsilon = \text{constant}$  curves are very far from those relevant to the isotropic case, especially when azimuth slopes are negligible with respect to range ones.

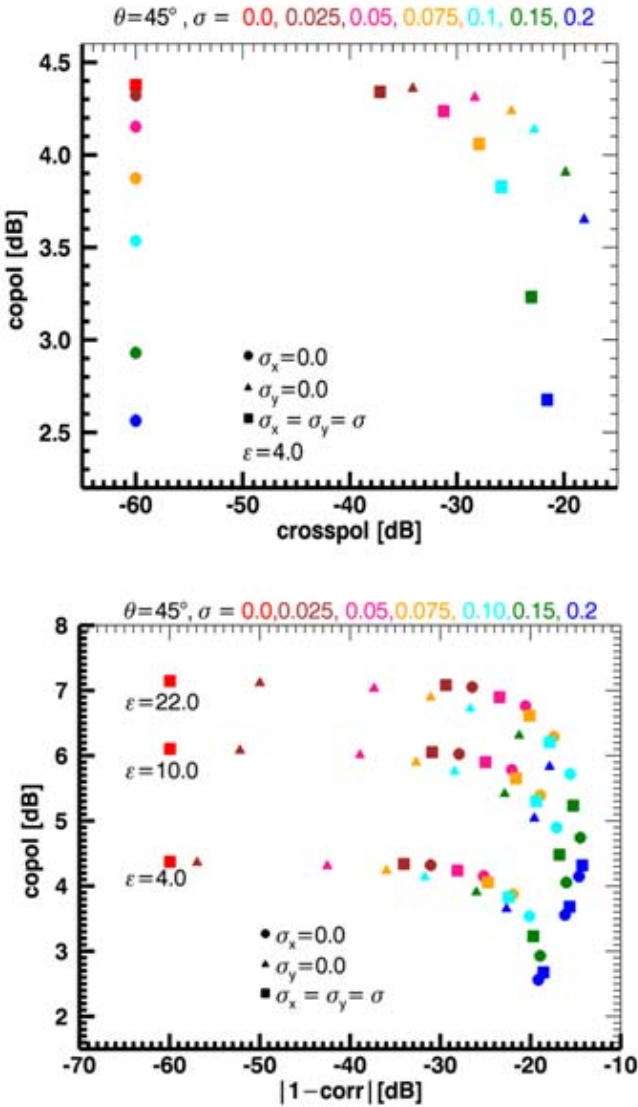


Fig.5. Copol-crosspol (top) and copol-corr graphs (bottom) for anisotropic analysis ( $\theta = 45^\circ$ ).

In Fig. 5(bottom) the results for the copol-corr graph are reported. When  $\sigma$  is equal to zero, corr is equal to one and, hence, (1-corr) is equal to zero: for visualization purposes in this case, we set (1-corr) to the conventional value of -60 dB. Due to the strong dependence of both copol ratio and corr on range slopes, we note that the graph relevant to the case of  $\sigma_x = 0$ , is similar to the one obtained for  $\sigma_x = \sigma_y = \sigma$ , whereas the graph relevant to the case of  $\sigma_y = 0$  significantly departs from the case  $\sigma_x = \sigma_y = \sigma$ . However, in this case we note that  $\varepsilon = \text{constant}$  curves in presence of anisotropy are very close to those relevant to the isotropic case. This is demonstrated by plotting the points relevant to different values of  $\varepsilon$ , which highlights how the estimation of  $\varepsilon$  is not significantly affected by anisotropic roughness. This is a very important result, suggesting that the use of copol-

corr graphs should be preferred for bare soil moisture retrieval, whenever uncontrollable anisotropies may be present in the macroscopic roughness.

#### 4. CONCLUSIONS

We present a fully polarimetric SAR simulator, which we named Pol-SARAS. It is based on the use of sound direct electromagnetic models and it is able to provide as output the simulated data of all the three polarization channels in such a way as to obtain the correct covariance or coherence matrixes on the final focused images. At the moment, the proposed simulator takes into account the surface scattering contribution only; however, thanks to the simulator modularity, volumetric and double-bounce contributions can be included, if reliable models are available.

Presented polarimetric simulator has been shown to provide coherency matrixes in agreement with theoretically expected ones. It will allow us checking the effects on polarimetric data of scene features also when they are not easy to be theoretically modeled, such as anisotropy of large-scale roughness, often present in ploughed agricultural fields.

#### 5. REFERENCES

- [1] J. S. Lee and E. Pottier, *Polarimetric Radar Imaging: From Basics to Applications*, CRC Press, Boca Raton (FL), 2009.
- [2] G. Franceschetti, M. Migliaccio, D. Riccio, and G. Schirinzi, "SARAS: a SAR raw signal simulator", *IEEE Trans. Geosc. Remote Sensing*, vol.30, pp.110-123, 1992.
- [3] S. Cimmino, G. Franceschetti, A. Iodice, D. Riccio, and G. Ruello, "Efficient Spotlight SAR Raw Signal Simulation of Extended Scenes", *IEEE Trans. Geosc. Remote Sensing*, vol.41, pp. 2329- 2337, 2003.
- [4] G. Franceschetti, R. Guida, A. Iodice, D. Riccio, and G. Ruello, "Efficient Simulation of Hybrid Stripmap/Spotlight SAR Raw Signal From Extended Scenes", *IEEE Transactions on Geoscience and Remote Sensing*, vol.42, no.11, pp. 2385-2396, 2004.
- [5] G. Franceschetti, A. Iodice, S. Perna, and D. Riccio, "SAR Sensor Trajectory Deviations: Fourier Domain Formulation and Extended Scene Simulation of Raw Signal", *IEEE Transactions on Geoscience and Remote Sensing*, vol.44, no.9, pp. 2323-2334, 2006.
- [6] A. Iodice, A. Natale, D. Riccio, "Polarimetric Two-Scale Model for Soil Moisture Retrieval via Dual-Pol HH-VV SAR Data", *IEEE Journal of Selected Topics in Applied Earth Observations and Remote Sensing*, vol.6, no.3, pp. 1163-1171, 2013.
- [7] I. Hajnsek, E. Pottier, and S. R. Cloude, "Inversion of surface parameters from polarimetric SAR," *IEEE Trans. Geosci. Remote Sens.*, vol. 41, no. 4, pp. 727-744, Apr. 2003.